

General Bianchi IX dynamics in bouncing braneworld cosmology: homoclinic chaos and the BKL conjecture

Rodrigo Maier¹, Ivano Damião Soares¹
and Eduardo Valentino Tonini²

¹ Centro Brasileiro de Pesquisas Físicas – CBPF, Rio de Janeiro, Brazil

² Instituto de Educação Tecnológica do Espírito – IFES, Vitória, Brazil

January 28, 2022

Abstract

In the framework of braneworld formalism, we examine the dynamics of a Bianchi IX model with three scale factors on a 4-dim Lorentzian brane embedded in a 5-dim conformally flat empty bulk with a timelike extra dimension. The matter content is a pressureless perfect fluid restricted to the brane. In this scenario Einstein's equations on the brane reduces to a 6-dim Hamiltonian dynamical system with additional terms – due to the bulk-brane interaction – that avoid the singularity and implement nonsingular bounces in the early phase of the universe. Due to an effective cosmological constant on the brane the phase space of the model presents two critical points (a saddle-center-center and a center-center-center) in a finite region of phase space, and two asymptotic de Sitter critical points at infinity, one acting as an attractor to late-time acceleration dynamics. The critical points belong to a 2-dim invariant plane; together they organize the dynamics of the phase space. The center-center-center critical point corresponds to a stable Einstein universe configuration with perpetually oscillatory orbits in its neighborhood. On the other hand the saddle-center-center engenders in the phase space the topology of stable and unstable 4-dim cylinders $R \times S^3$, where R is a saddle direction and S^3 is the center manifold of unstable periodic orbits,

the latter being the nonlinear extension of the center-center sector. By a proper canonical transformation we are able to separate the three degrees of freedom of the dynamics into one degree connected with the expansion and/or contraction of the scales of the model, and two pure rotational degrees of freedom associated with the center manifold S^3 . It follows that the typical dynamical flow is an oscillatory mode about the orbits of the invariant plane. For the stable and unstable cylinders we have the oscillatory motion about the separatrix towards the bounce, leading to the homoclinic transversal intersection of the cylinders, as shown numerically in two distinct experiments. We show that the homoclinic intersection manifold has the topology of $R \times S^2$ consisting of homoclinic orbits biasymptotic to the center manifold S^3 . This behavior defines a *chaotic saddle* associated with S^3 , indicating that the intersection points of the cylinders have the nature of a Cantor set with a compact support S^2 . This is an invariant signature of chaos in the model. We discuss the possible connection between these properties of the dynamics, namely the oscillatory approach to the bounce together with its chaotic behavior, and analogous features present in the BKL conjecture in general relativity.

PACS numbers: 05.45.-a, 05.45.Pq, 98.80.-k, 11.25.-w

1 Introduction

The general Bianchi IX model has become a paradigm for the behavior of the general relativity dynamics near the cosmological singularity since the seminal papers of Belinskii, Khalatnikov and Lifshitz (BKL)[1, 2, 3], and collaborators[4, 5]. They showed that in a Bianchi IX model with three scale factors the approach to the singularity ($t \rightarrow 0$) is an oscillatory mode, consisting of an infinite sequence of Kasner eras in each of which two of the scale factors oscillate while the third decreases monotonically. On passing from one era to another (with decreasing time t) the monotonic behavior is transferred to another of the three scale factors. It was also shown that (i) the length of each era was determined by a sequence of numbers x_s , $0 < x_s < 1$, $s = \text{integer}$, each of which arises from the preceding one by the map $x_{s+1} = \text{the fractional part of } 1/x_s$, with the length of the s -th era given by $k_s = \text{the integral part of } 1/x_s$; (ii) this map leads to spontaneous stochastization in the sequence of eras on approaching the singularity ($t \rightarrow 0$) for arbitrary initial conditions given at $t > 0$. Due to the involved nonintegrable dynamics the evolution of the model had to be actually treated in asymptotic

regions of arbitrarily small times together with truncations made to guarantee the validity of the perturbation method, so that “in the most general case all details of such regime are not yet fully understood”[1]. In the past four decades the dynamics of these models has been reexamined in an extensive literature but – as in the BKL work – the approach has been basically twofold: to obtain maps which approximate the dynamics and which exhibit strong stochastic properties, and the discussion of how well these discrete maps represent the full nonlinear dynamics of Bianchi IX models in general relativity. From the point of view of the phase space flow the interest in the chaoticity of Bianchi IX models has been mainly focused on the mixmaster universe (the vacuum Bianchi IX case with three scale factors), although the question of the behavior (chaotic or not) remained unsettled mainly due to the absence of an invariant characterization of chaos in the model (standard chaotic indicators as Liapunov exponents being coordinate dependent and hence questionable). Therefore, along with the Cosmic Censorship Conjecture, the BKL conjecture is probably one of the major unsolved issues of classical general relativity connected to the presence of a singularity in the dynamics.

Our purpose in the present paper is to examine the dynamics of a 4-dim Bianchi IX model with three scale factors in the framework of a braneworld formalism (which encompasses general relativity as a classical low-energy limit). Due to an extra timelike dimension brane-bulk interaction terms correct general relativity substituting the singularity by nonsingular bounces in the cosmological dynamics. The dynamics of the approach to the bounces is extremely complex presenting oscillatory and chaotic features of the BKL-type but, as we will show, they are amenable to an exact analytical/numerical treatment so that we may have a more clear picture of what happens in the general relativity limit.

Most of the approaches to the problem of the initial singularity and to the possible solutions adopted to circumvent this problem lie in the realm of a quantum theory of gravitation. In fact we may consider that the initial conditions of our present expanding Universe were fixed when the early Universe emerged from a Planckian regime and started its classical evolution. However, by evolving back the initial conditions using Einstein’s classical equations the Universe is driven toward a singular point where the classical regime is no longer valid[6]. This is an indication that classical general relativity is not a complete theory and in this domain quantum processes must be taken into account.

Among several propositions to describe the dynamics in the semiclassical domain prior to the classical regime are, for instance, quantum loop cosmology[7] and the string based formalism of D-branes[8], both of them leading to corrections in Einstein's equations and encompassing general relativity as a classical (low energy) limit. In the present paper we adhere to the so-called braneworld scenario[9]-[10] based on the string formalism of D-branes. In this context, extra dimensions are introduced by a bulk space and all the matter in the Universe would be trapped on a brane embedded in the bulk with three spatial dimensions; only gravitons would be allowed to leave the brane and move into the full bulk[11]. At low energies general relativity is recovered but at high energies significant changes are introduced in the gravitational dynamics. Our interest in this framework comes from the fact that it can provide corrections that are dominant in the neighborhood of the singularity, resulting in a repulsive force which avoids it completely and leads the Universe to undergo nonsingular bounces. Bouncing brane world models were constructed by Shtanov and Sahni[10] based upon a Randall-Sundrum type action with one extra timelike dimension. A complete analysis of bouncing brane world dynamics embedded in a five-dimensional de Sitter spacetime may be found in Refs. [12, 13], where both high energy local corrections as well as nonlocal bulk corrections are analyzed on a spatially homogeneous brane.

Although spacelike extra dimensions theories have received more attention in the last decades[11], studies regarding extra timelike dimensions have been considered[14, 15, 16, 17]. Albeit presenting some problematic issues[18, 19] it has been shown[20] that they might be circumvented by considering a noncompact timelike extra dimension, which is the case of the model in this paper.

In our braneworld scenario we consider a 5-dim de Sitter bulk space with a timelike extra dimension, and a 4-dim Lorentzian brane with a Bianchi IX geometry with three scale factors. The matter content of the model is taken as a pressureless perfect fluid (dust) restricted to the brane and an effective nonvanishing cosmological constant is also considered. With the above assumptions we show that the Gauss-Codazzi equations, and hence, the modified field equations on the brane are automatically satisfied. The modified Einstein's equations for the model have a first integral that can be expressed as a Hamiltonian constraint, yielding a three degrees of freedom dynamical system in a 6-dim phase space. The additional correction terms due to the bulk-brane interaction avoid the initial singularity resulting in-

stead to nonsingular bounces in the model. One of the main features of the phase space is the presence of a saddle-center-center critical point with an associated center manifold of unstable periodic orbits having the topology S^3 . We will show that from the center manifold it emerges stable and unstable manifolds with the topology of spherical cylinders $R \times S^3$ (constituted actually of bounded oscillatory orbits) which cross each other transversally in the neighborhood of the bounces. These transversal crossings provide an invariant characterization of homoclinic chaos in the model.

These results are in realm of recent studies in the characterization of homoclinic chaos for Hamiltonian dynamical systems with $n \geq 2$ degrees of freedom. For $n = 2$ the characterization of chaos connected with the presence of homoclinic phenomena in the dynamics has been the object of an extensive outstanding literature (cf. [21, 22, 23, 24, 25, 26] and references therein). The dynamics near homoclinic orbits is very complex, with the homoclinic intersection manifold associated with the presence of the well-known horseshoe structures (cf. [27, 28, 29] and references therein), which is an invariant signature of chaos. Furthermore, invariant Cantor sets associated with a horseshoe construction are connected to chaotic saddles[30]-[32]. For $n \geq 2$ orbits homoclinic to the center manifold are expected to exist. It has been shown, for instance, that critical points of the type saddle-center-...-center induce reaction type dynamics in the framework of Transition State Theory (see [33] and references therein). The existence of such homoclinic orbits has been studied in [33, 34]. Although there are no theorems describing the dynamics connected with orbits homoclinic to S^3 , it has been shown[35] that if there is a transversal intersection of the stable and unstable manifolds, a chaotic saddle, and hence an homoclinic trajectory must exist. An interesting analysis of this feature was given in [34], where the authors provide a computational procedure to detect a chaotic saddle (and thus homoclinic orbits) in the case of Hamiltonian systems with three degrees of freedom. In the present paper we follow an alternative procedure to show the presence of homoclinic connections with the center manifold S^3 .

We organize the paper as follows. In the next section we present a brief introduction to BraneWorld Theory, deriving the modified field equations on the brane. In Section III we construct a general Bianchi IX cosmological brane model, with an effective cosmological constant and the matter content being dust. In Section IV we study the structure of the phase space, identifying the constants for the linearized motion. In Section V the dynamics about the saddle-center-center critical point is examined. Section VI is devoted to

a complete analysis of the nonlinear center manifold, together with the 4-dim stable and unstable cylinders that emanate from it. Finally in Section VII we study the homoclinic transversal intersections of the cylinders that gives an invariant characterization of chaos in the dynamics. Conclusions and future perspectives are presented in the final section.

2 The field equations

For sake of completeness we give here a brief introduction to Braneworld Theory, making explicit the specific assumptions used to obtain the dynamics of the model. We refer to [10, 11] for a more complete and detailed discussion and our notation closely follows [6]. We start with a 4-D Lorentzian brane Σ with metric $^{(4)}g_{ab}$, embedded in a 5-D conformally flat bulk \mathcal{M} with metric $^{(5)}g_{AB}$. Capital Latin indices run from 0 to 4, small Latin indices run from 0 to 3. We regard Σ as a common boundary of two pieces \mathcal{M}_1 and \mathcal{M}_2 of \mathcal{M} and $^{(4)}g_{ab}$ is the induced geometry on the brane by the metrics of the two pieces. These metrics should coincide on Σ although the extrinsic curvatures of Σ with respect to \mathcal{M}_1 and \mathcal{M}_2 can be different. The action for the theory has the general form

$$\begin{aligned}
S = & \frac{1}{2\kappa_5^2} \left\{ \int_{M_1} \sqrt{-\epsilon} {}^{(5)}g \left[{}^{(5)}R - 2\Lambda_5 + 2\kappa_5^2 L_5 \right] d^5x \right. \\
& + \int_{M_2} \sqrt{-\epsilon} {}^{(5)}g \left[{}^{(5)}R - 2\Lambda_5 + 2\kappa_5^2 L_5 \right] d^5x \\
& + 2\epsilon \int_{\Sigma} \sqrt{-{}^{(4)}g} K_2 d^4x - 2\epsilon \int_{\Sigma} \sqrt{-{}^{(4)}g} K_1 d^4x \Big\} \\
& + \frac{1}{2} \int_{\Sigma} \sqrt{-{}^{(4)}g} \left(\frac{1}{2\kappa_4^2} {}^{(4)}R - 2\sigma \right) d^4x \\
& + \int_{\Sigma} \sqrt{-{}^{(4)}g} L_4({}^{(4)}g_{ab}, \rho) d^4x .
\end{aligned} \tag{1}$$

In the previous equation, ${}^{(5)}R$ is the Ricci scalar of the Lorentzian 5-D metric $^{(5)}g_{AB}$ on \mathcal{M} , and ${}^{(4)}R$ is the scalar curvature of the induced metric $^{(4)}g_{ab}$ on Σ . The parameter σ denotes the brane tension. The unit vector n^A is normal to the boundary Σ and has norm ϵ . If $\epsilon = +1$ the signature of the bulk space is $(+, +, -, -, -)$, so that the extra dimension is timelike. The quantity

$K = K_{ab}^{(4)} g^{ab}$ is the trace of the symmetric tensor of extrinsic curvature $K_{ab} = Y_{,a}^C Y_{,b}^D \nabla_C n_D$, where $Y^A(x^a)$ are the embedding functions of Σ in \mathcal{M} [36]. While $L_4^{(4)}(g_{ab}, \rho)$ represents the Lagrangian density of the perfect fluid[37] (with equation of state $p = \alpha\rho$), whose dynamics is restricted to the brane Σ , L_5 denotes the Lagrangian of matter in the bulk. All integrations over the bulk and the brane are taken with the natural volume elements $\sqrt{-\epsilon^{(5)} g} d^5x$ and $\sqrt{-^{(4)}g} d^4x$ respectively. Einstein constants in five- and four-dimensions are indicated with κ_5^2 and $\kappa_4^2 \equiv 8\pi G_N$, respectively (G_N being the Newton's constant on the brane). Throughout this section we use natural units with $\hbar = c = 1$.

Variations that leave the induced metric on Σ intact, furnish the equations

$$^{(5)}G_{AB} + \Lambda_5 ^{(5)}g_{AB} = \kappa_5^2 ^{(5)}T_{AB} . \quad (2)$$

Considering arbitrary variations of $^{(5)}g_{AB}$ and taking into account Eq. (2), we obtain

$$^{(4)}G_{ab} + \epsilon \frac{\kappa_4^2}{\kappa_5^2} \left(S_{ab}^{(1)} + S_{ab}^{(2)} \right) = \kappa_4^2 (\tau_{ab} - \sigma g_{ab}) , \quad (3)$$

where $S_{ab} \equiv K_{ab} - K^{(4)}g_{ab}$, and τ_{ab} is the energy momentum tensor on the brane. In the limit $\kappa_4^2 \gg \kappa_5^2$, Eq. (3) reduces to the Israel-Darmois junction conditions[38]

$$\left(S_{ab}^{(1)} + S_{ab}^{(2)} \right) = \epsilon \kappa_5^2 (\tau_{ab} - \sigma^{(4)}g_{ab}) . \quad (4)$$

Imposing the Z_2 -symmetry[11] and using the junction conditions (Eq. 4), we determine the extrinsic curvature on the brane,

$$K_{ab} = \frac{\epsilon}{2} \kappa_5^2 \left[\left(\tau_{ab} - \frac{1}{3} \tau^{(4)} g_{ab} \right) + \frac{\sigma}{3} g_{ab} \right] . \quad (5)$$

Now using Gauss equation

$$\begin{aligned} ^{(4)}R_{abcd} = & ^{(5)}R_{MNRs} Y_{,a}^M Y_{,b}^N Y_{,c}^R Y_{,d}^S - \\ & \epsilon (K_{ac} K_{bd} - K_{ad} K_{bc}) , \end{aligned} \quad (6)$$

together with Eqs. (2) and (5) we obtain the induced field equations on the brane

$$\begin{aligned} ^{(4)}G_{ab} + \Lambda_4 ^{(4)}g_{ab} = & 8\pi G_N \tau_{ab} - \epsilon \kappa_5^4 \Pi_{ab} + \\ & \epsilon E_{ab} + \epsilon F_{ab} . \end{aligned} \quad (7)$$

In the above $E_{ab} = {}^{(5)}C_{ABCD}n^A Y_{,a}^B n^C Y_{,b}^D$ is the projection of the 5-D Weyl tensor, and we have defined

$$\Lambda_4 = \frac{1}{2}\kappa_5^2 \left(\frac{\Lambda_5}{\kappa_5^2} - \frac{1}{6}\epsilon\kappa_5^2\sigma^2 \right), \quad (8)$$

$$G_N = \epsilon \frac{\kappa_5^4 \sigma}{48\pi}, \quad (9)$$

$$\begin{aligned} \Pi_{ab} = & -\frac{1}{4}\tau_a^c \tau_{bc} + \frac{1}{12}\tau\tau_{ab} + \frac{1}{8}{}^{(4)}g_{ab}\tau^{cd}\tau_{cd} - \\ & \frac{1}{24}\tau^2{}^{(4)}g_{ab}, \end{aligned} \quad (10)$$

$$\begin{aligned} F_{ab} = & \frac{2}{3}\kappa_5^2 \left\{ \epsilon {}^{(5)}T_{BD}Y_{,a}^B Y_{,b}^D - \right. \\ & \left. \left[{}^{(5)}T_{BD}n^B n^D + \frac{1}{4}\epsilon {}^{(5)}T \right] {}^{(4)}g_{ab} \right\}, \end{aligned} \quad (11)$$

Here we stress that the effective 4-dim cosmological constant can be set to zero in the present case of an extra timelike dimension by properly fixing the bulk cosmological constant as $\Lambda_5 = \frac{1}{6}\kappa_5^4 \sigma^2$. It is important to notice that for a 4-dim brane embedded in a conformally flat empty bulk we have the absence of the Weyl conformal tensor projection E_{ab} , and of F_{ab} in Eq. (7).

On the other hand, Codazzi's equations imply that

$$\nabla_a K - \nabla_b K_a^b = \frac{1}{2}\epsilon\kappa_5^2 \nabla_b \tau_a^b. \quad (12)$$

By imposing that $\nabla_b \tau_a^b = 0$, the Codazzi conditions read

$$\nabla^a E_{ab} = \kappa_5^4 \nabla^a \Pi_{ab} + \nabla^a F_{ab}. \quad (13)$$

where ∇_a is the covariant derivative with respect to the induced metric ${}^{(4)}g_{ab}$. Eqs. (7) and (13) are the dynamical equations of the gravitational field on the brane. In the following section we drop the index (4) in the geometrical quantities on the brane.

3 The model

Let us consider a Bianchi IX spatially homogeneous geometry on the four-dimensional brane embedded in a five-dimensional, conformally flat and empty

bulk ($E_{ab} = 0 = F_{ab}$) with a timelike extra dimension ($\epsilon = 1$). In comoving coordinates on the brane, the line element can be expressed as

$$ds^2 = dt^2 - (\theta^1)^2 - (\theta^2)^2 - (\theta^3)^2, \quad (14)$$

where t is the cosmological time and

$$\theta^1 = M(t) \omega^1, \quad \theta^2 = N(t) \omega^2, \quad \theta^3 = R(t) \omega^3. \quad (15)$$

Here $M(t)$, $N(t)$ and $R(t)$ are the scale factors of the model and the ω^i ($i = 1, 2, 3$) are Bianchi-type IX 1-forms satisfying

$$d\omega^i = \frac{1}{2} \epsilon^{ijk} \omega^j \wedge \omega^k, \quad (16)$$

where d denotes the exterior derivative.

The matter content of the model is assumed to be dust, whose energy density ρ is measured by the comoving observers with 4-velocity $u^a = \delta_0^a$. By imposing that the energy-momentum tensor of dust,

$$\tau^{ab} = \rho u^a u^b, \quad (17)$$

is conserved separately, namely $\nabla_a \tau^{ab} = 0$, we obtain

$$\rho = \frac{C_0}{MNR}, \quad (18)$$

where C_0 is a constant of motion connected to the dust energy. The components of tensor Π_{ab} are given by

$$\Pi_{ab} = \frac{1}{12} \rho^2 g_{ab}, \quad (19)$$

so that Codazzi's equations,

$$\nabla_a \Pi^{ab} = 0, \quad (20)$$

are identically satisfied. Therefore, Eq. (7) reduces to

$$G_{ab} + \Lambda g_{ab} = 8\pi G_N \tau_{ab} - \kappa_5^4 \Pi_{ab}, \quad (21)$$

which are the modified Einstein's field equations for the model. As the Gauss-Codazzi equations are automatically satisfied via (20) and (21), the

assumption of a conformally flat empty bulk is consistent. We also see that as $\epsilon = 1$ (a timelike extra dimension) the term Π_{ab} in (21) acts as a potential barrier to the dynamics avoiding the singularity.

In terms of the metric functions (14) equations (21) correspond to the modified Friedmann's equations of the model, having a first integral that can be expressed as the Hamiltonian constraint

$$\begin{aligned}
H &= \frac{1}{8} \left(-\frac{M}{NR} p_M^2 - \frac{N}{MR} p_N^2 - \frac{R}{MN} p_R^2 + \frac{2}{M} p_N p_R + \frac{2}{N} p_M p_R + \frac{2}{R} p_M p_N \right) \\
&+ \frac{1}{2MNR} [M^4 + N^4 + R^4 - (M^2 - N^2)^2 - (R^2 - M^2)^2 - (R^2 - N^2)^2] \\
&- 2\Lambda MNR - 2E_0 + \kappa^2 \frac{E_0^2}{MNR} = 0
\end{aligned} \tag{22}$$

where p_M , p_N and p_R are the momenta canonically conjugate to M , N and R , respectively. $E_0 \equiv 8\pi G_N C_0$ and $\kappa^2 \equiv (8\pi G_N)^{-1} |\sigma|^{-1}$. From Hamilton's equations we obtain the following dynamical system

$$\begin{aligned}
\dot{M} &= \frac{\partial H}{\partial p_M} = \frac{1}{4} \left(\frac{p_N}{R} + \frac{p_R}{N} - \frac{M}{NR} p_M \right), \\
\dot{N} &= \frac{\partial H}{\partial p_N} = \frac{1}{4} \left(\frac{p_M}{R} + \frac{p_R}{M} - \frac{N}{MR} p_N \right), \\
\dot{R} &= \frac{\partial H}{\partial p_R} = \frac{1}{4} \left(\frac{p_M}{N} + \frac{p_N}{M} - \frac{R}{MN} p_R \right), \\
\dot{p}_M &= -\frac{\partial H}{\partial M} = \frac{1}{8} \left(\frac{p_M^2}{NR} - \frac{N}{M^2 R} p_N^2 - \frac{R}{M^2 N} p_R^2 + \frac{2}{M^2} p_N p_R \right) \\
&+ \frac{1}{2M^2 NR} [M^4 + N^4 + R^4 - (R^2 - N^2)^2 - (R^2 - M^2)^2 - (M^2 - N^2)^2] \\
&+ 2\Lambda NR - \frac{2}{MNR} [M^3 + M(R^2 - M^2) - M(M^2 - N^2)] + \frac{\kappa^2 E_0^2}{M^2 NR}, \\
\dot{p}_N &= -\frac{\partial H}{\partial N} = \frac{1}{8} \left(\frac{p_N^2}{MR} - \frac{M}{N^2 R} p_M^2 - \frac{R}{MN^2} p_R^2 + \frac{2}{N^2} p_M p_R \right) \\
&+ \frac{1}{2MN^2 R} [M^4 + N^4 + R^4 - (R^2 - N^2)^2 - (R^2 - M^2)^2 - (M^2 - N^2)^2] \\
&+ 2\Lambda MR - \frac{2}{MNR} [N^3 + N(R^2 - N^2) - N(N^2 - M^2)] + \frac{\kappa^2 E_0^2}{MN^2 R},
\end{aligned}$$

$$\begin{aligned}
\dot{p}_R = & -\frac{\partial H}{\partial R} = \frac{1}{8} \left(\frac{p_R^2}{MN} - \frac{M}{NR^2} p_M^2 - \frac{N}{MR^2} p_N^2 + \frac{2}{R^2} p_M p_N \right) \\
& + \frac{1}{2MNR^2} [M^4 + N^4 + R^4 - (R^2 - N^2)^2 - (R^2 - M^2)^2 - (M^2 - N^2)^2] \\
& + 2\Lambda MN - \frac{2}{MNR} [R^3 + R(M^2 - R^2) - R(R^2 - N^2)] + \frac{\kappa^2 E_0^2}{MNR^2}. \quad (23)
\end{aligned}$$

Equations (22) and (23) are equivalent to the modified field equations (21).

4 The structure of the phase space

In this section we will examine the basic structures that organize the dynamics of the system in the phase space. The first of these are the set of critical points of the system given, from Eqs. (23)), by $M = N = R = M_0$ and $p_M = p_N = p_R = 0$, where M_0 satisfies the equation

$$M_0^6 - \frac{M_0^4}{4\Lambda} + \kappa^2 \frac{E_{\text{cr}}^2}{2\Lambda} = 0. \quad (24)$$

We can observe that the critical points, determined by the positive real roots of (24), depend on their respective critical energy appearing in the third term of the left-hand-side of the equation, as a consequence of the bulk-brane interaction.

We must also consider the further relation

$$\frac{3}{2}M_0 + \kappa^2 \frac{E_{\text{cr}}^2}{M_0^3} - 2\Lambda M_0^3 - 2E_{\text{cr}} = 0, \quad (25)$$

obtained by evaluating the Hamiltonian constraint (22) at the critical points. Solving (25) for E_{cr} we will restrict ourselves to the root

$$E_{\text{cr}} = \frac{M_0^3}{\kappa^2} \left(1 - \sqrt{1 - \frac{3\kappa^2}{2M_0^2} + 2\kappa^2\Lambda} \right) \quad (26)$$

which yields the correct result in the general relativity limit[39] ($\kappa^2 \rightarrow 0$ or equivalently $|\sigma| \rightarrow \infty$). Combining Eqs. (24) and (26) we obtain for the critical points the two real positive solutions

$$M_{0,2} = \frac{\kappa (3 \pm \sqrt{1 - 16\kappa^2\Lambda})}{2(1 + 2\kappa^2\Lambda) \sqrt{(1 - 4\kappa^2\Lambda \pm \sqrt{1 - 16\kappa^2\Lambda}) / (1 + 2\kappa^2\Lambda)}} \quad (27)$$

with $M_{0_1} \leq M_{0_2}$. The equality occurs for $\Lambda = 1/16\kappa^2$, the case of just one critical point; for $\Lambda > 1/16\kappa^2$ no critical points exist. In the following we are going to restrict ourselves to the case $\Lambda < 1/16\kappa^2$. As we will see, this condition is necessary for the presence of homoclinic orbits that establish the chaotic behavior of the dynamics. The respective energies associated with the critical points are obtained by substituting $M_{0_{1,2}}$ in (26) yielding

$$E_{\text{cr}(1,2)} = \frac{\kappa (3 \pm \sqrt{1 - 16\kappa^2\Lambda})^2}{8 (1 + 2\kappa^2\Lambda)^{3/2} \sqrt{1 - 4\kappa^2\Lambda \pm \sqrt{1 - 16\kappa^2\Lambda}}}. \quad (28)$$

Much of our understanding of nonlinear systems derives from the linearization about critical points and from the determination of existing invariant submanifolds, which are structures that organize the dynamics in phase space. The system under examination here presents a two-dimensional invariant manifold of the dynamics defined by

$$p_M = p_N = p_R, \quad M = N = R. \quad (29)$$

This invariant plane is actually the intersection of two four-dimensional invariant submanifolds, defined by $(M = N, p_M = p_N)$ and $(N = R, p_N = p_R)$. The critical points obviously belong to the invariant plane.

Finally a straightforward analysis of the infinity of the phase space shows that it has two critical points in this region, one acting as an attractor (stable de Sitter configuration) and the other as a repeller (unstable de Sitter configuration). The scale factors M , N and R approach the de Sitter attractor as $M = N = R \sim \exp(\sqrt{\Lambda/3} t)$, so that the two de Sitter configurations also belong to the invariant plane. The phase picture of the invariant plane is displayed in Fig. 1, in the variables (x, p_x) defined in section 5.

To proceed let us now linearize the dynamical equations (23) about the critical points $(M = N = R = M_{0_i}, p_M = p_N = p_R = 0)$, $i = 1, 2$. Defining

$$\begin{aligned} X &= (M - M_{0_i}), & W &= (p_M - 0), \\ Y &= (N - M_{0_i}), & K &= (p_N - 0), \\ Z &= (R - M_{0_i}), & L &= (p_R - 0), \end{aligned} \quad (30)$$

we obtain

$$\begin{pmatrix} \dot{X} \\ \dot{Y} \\ \dot{Z} \\ \dot{W} \\ \dot{K} \\ \dot{L} \end{pmatrix} = \begin{pmatrix} 0 & 0 & 0 & -\alpha & \alpha & \alpha \\ 0 & 0 & 0 & \alpha & -\alpha & \alpha \\ 0 & 0 & 0 & \alpha & \alpha & -\alpha \\ \beta & \gamma & \gamma & 0 & 0 & 0 \\ \gamma & \beta & \gamma & 0 & 0 & 0 \\ \gamma & \gamma & \beta & 0 & 0 & 0 \end{pmatrix} \begin{pmatrix} X \\ Y \\ Z \\ W \\ K \\ L \end{pmatrix} \quad (31)$$

where

$$\begin{aligned} \alpha &= \frac{1}{4M_{0i}}, \quad \beta = \frac{3}{M_{0i}} - \frac{2\kappa^2 E_{\text{cr}(i)}^2}{M_{0i}^5}, \\ \gamma &= 2\Lambda M_{0i} - \frac{3}{2M_{0i}} - \frac{\kappa^2 E_{\text{cr}(i)}^2}{M_{0i}^5}. \end{aligned} \quad (32)$$

The associated characteristic polynomial results

$$\begin{aligned} P(\lambda) &= (\lambda - \sqrt{2\gamma\alpha + \beta\alpha})(\lambda + \sqrt{2\gamma\alpha + \beta\alpha}) \\ &\times (\lambda - \sqrt{2\alpha(\gamma - \beta)})^2 (\lambda + \sqrt{2\alpha(\gamma - \beta)})^2, \end{aligned} \quad (33)$$

with roots

$$\lambda_{(i)} = \pm i \frac{\sqrt{2}}{M_{0i}}, \quad (34)$$

$$\lambda_{(i)} = \pm \sqrt{3\Lambda - \frac{1}{2M_{0i}^2}}, \quad (35)$$

where (24) was used. The pair of imaginary eigenvalues (34) has multiplicity two, characterizing a center-center structure. The analysis of the center-center structure will reveal a manifold of linearized unstable periodic orbits with the topology of S^3 . The extension of this manifold to the nonlinear domain constitutes the center manifold[31, 22] of unstable periodic orbits, parametrized with the constant of motion E_0 (with $E_0 < E_{\text{cr}}$), which will play a central role in our discussions in the next section.

Using (25) and (27) one can show that the pair of eigenvalues (35) are imaginary for the critical point $i = 1$ and real for the critical point $i = 2$. As we shall see below, we have (in the latter case $i = 2$) that the critical point P_2

is a saddle-center-center about which the dynamics has the topology $R \times S^3$. On the other hand, the critical point P_1 is a center-center-center critical point, about which the dynamics has the topology $S^1 \times S^3$ corresponding to perpetually oscillatory Bianchi IX universes.

Finally we should note that, in the limit case of a single critical point (when $16\kappa^2\Lambda = 1$), the second pair of eigenvalues (35) are zero and no saddle structure is present in the dynamics. The analysis of this case will not be undertaken here. In the remaining of this section our discussion follows the lines of [39] done for the general relativity case.

To display the structure of the linearized motion, we start by diagonalizing the linearization matrix of (31) with the use of a similarity transformation \mathfrak{R} whose columns are composed of six independent eigenvectors of the linearization [40]. A judicious choice of \mathfrak{R} yields primed variables defined by the transformation

$$\begin{aligned} X' &= \frac{1}{3} (X + Y + Z), \\ Y' &= \frac{1}{M_{0_i}} (X - Y), \\ Z' &= \frac{1}{M_{0_i}} (X + Y - 2Z), \\ W' &= (W + K + L), \\ K' &= \frac{M_{0_i}}{2} (W - K), \\ L' &= \frac{M_{0_i}}{6} (W + K - 2L). \end{aligned} \tag{36}$$

In these new variables, the quadratic Hamiltonian about the i -th critical point is expressed in the form

$$\begin{aligned} H &= \frac{1}{4} \left(\frac{1}{6} W'^2 - 6qX'^2 \right) - \left(\frac{1}{2M_{0_i}^3} K'^2 + M_{0_i} Y'^2 \right) \\ &- \left(\frac{3}{2M_{0_i}^3} L'^2 + \frac{M_{0_i}}{3} Z'^2 \right) + 2(E_{\text{cr}(i)} - E_0), \end{aligned} \tag{37}$$

where

$$q = 6(\Lambda M_{0_i} - \kappa^2 E_{\text{cr}(i)}^2 / M_{0_i}^5). \tag{38}$$

These primed variables are conjugated to the pairs according to $[X', W'] = 1$, $[Y', K'] = 1$, $[Z', L'] = 1$, other Poisson brackets (PB) zero. The Hamiltonian (37) is separable, and we can identify the following constants of the linearized motion

$$E_q = \frac{1}{4} \left(\frac{1}{6} W'^2 - 6q X'^2 \right), \quad (39)$$

$$E_{rot1} = \frac{1}{2M_{0i}^3} K'^2 + M_{0i} Y'^2, \quad (40)$$

$$E_{rot2} = \frac{3}{2M_{0i}^3} L'^2 + \frac{M_{0i}}{3} Z'^2, \quad (41)$$

$$Q_1 = \frac{M_{0i}}{3} Y' Z' + \frac{1}{2M_{0i}^3} K' L', \quad (42)$$

$$Q_2 = \frac{1}{2M_{0i}} \left(L' Y' - \frac{1}{3} K' Z' \right), \quad (43)$$

in the sense that they all have zero PB (37). The first three constants appear as separable pieces in the Hamiltonian (37).

The case of E_q demands a separate analysis for the two critical points. From previous relations we have that $q > 0$ for the critical point P_2 , so that E_q corresponds to the energy associated with the motion in the saddle sector. We remind that this is connected to the fact that the second pair of eigenvalues (35) are real for P_2 . For the critical point P_1 in which $q < 0$, E_q corresponds to the rotational energy in the additional rotational sector of the dynamics about P_1 which has the structure $S^1 \times S^3$ as mentioned already. The center-center-center critical point P_1 corresponds to a stable Einstein universe configuration with perpetually oscillatory orbits in its neighborhood.

In the following our focus will be the dynamical phenomena connected to the presence of the saddle-center-center critical point P_2 in the phase space of the model. We remark however that the analysis of the center manifold of unstable periodic orbits can also be applied to the case of the critical point P_1 .

5 The dynamics about the saddle-center-center critical point

We will now proceed to describe the topology of the general dynamics in the linear neighborhood of the saddle-center-center critical point P_2 for which $q > 0$.

If $E_q = 0$ two possibilities arise. The first possibility is $W' = 0 = X'$. The total energy in this case is $E_{rot1} + E_{rot2}$, the sum of the energies of the rotational motion in the linear neighborhood of the center-center manifold, corresponding to the motion on 2-dim tori[21]. The remaining two constants Q_1 and Q_2 are additional symmetries that arise due to the multiplicity two of the imaginary eigenvalues and are connected to the fact that the linearized dynamics in the center-center sector is that of a 2-dim isotropic harmonic oscillator. They are not all independent but related by

$$4E_{rot1}E_{rot2} = 12Q_1^2 + 6Q_2^2. \quad (44)$$

The motion in the constant energy surfaces $W' = 0 = X'$ are periodic orbits of the 2-dim isotropic harmonic oscillator, with Hamiltonian

$$\begin{aligned} H &= \left(\frac{1}{2M_{0_i}^3} K'^2 + M_{0_i} Y'^2 \right) + \left(\frac{3}{2M_{0_i}^3} L'^2 + \frac{M_{0_i}}{3} Z'^2 \right) \\ &- 2(E_{cr(i)} - E_0) = 0. \end{aligned} \quad (45)$$

The above equation shows that $E_0 - E_{cr} < 0$ is necessary for the dynamics in the rotational sector, defining a condition for the existence of the center-center manifold of periodic orbits.

By a proper canonical rescaling of the variables in (45) we can see that these constant energy surfaces are hyperspheres and that the constants of motion Q_1 , Q_2 and $Q_3 = E_{rot1} - E_{rot2}$ satisfy the algebra of the 3-dim rotation group under the PB operation, namely,

$$[Q_i, Q_j] = \epsilon^{ijk} Q_k. \quad (46)$$

The constant of motion Q_1 considered as a generator of infinitesimal contact transformations has a peculiar significance in characterizing the topology of the underlying group of the algebra (46). While Q_2 generates infinitesimal rotation of the orbits, Q_1 generates infinitesimal changes in eccentricity. The action of Q_1 is to take an orbit – let us say nearly circular – and to transform

it into an orbit of higher and higher eccentricity until it collapses into a straight line. Continued application of Q_1 produces again an elliptic orbit, but now traversed in the opposite sense, so that it takes a 720° to bring the orbit back into itself. The two-valuedness of the mapping arises from the fact that the orbits are oriented. Therefore the group generated by these constants of motion is homomorphic to the unitary unimodular group[41] so that the topology of the center-center manifold is in fact S^3 .

Due to the separate conservation of E_{rot_1} and E_{rot_2} (cf. (45)) one can show that the center manifold in the linear neighborhood of the critical points is foliated by Clifford 2-dim surfaces in S^3 [42], namely, 2-tori \mathfrak{S}_{E_0} contained in the energy surface $E_0 = \text{const}$. Such surfaces, as well as the S^3 manifold containing them, depend continuously on the parameter E_0 . We remark that these two tori will have limiting configurations $E_{rot_1} = 0$ or $E_{rot_2} = 0$, and correspond to the case of maximum eccentricity (for instance, a straight line in the plane (Y', Z')).

The second possibility to be considered is $W' = \pm 6\sqrt{q}X'$. It defines the linear stable V_S and unstable V_U manifolds of the saddle sector. V_S and V_U limit regions I ($E_q \equiv E_{hyp} < 0$) and regions II ($E_q \equiv E_{hyp} > 0$) of motion on hyperbolae which are solutions in the separable saddle sector $E_{hyp} = \frac{1}{4}(\frac{1}{6}W'^2 - 6qX'^2)$. Note that the saddle sector depicts the structure of the neighborhood of P_2 in Fig. 1, with V_U and V_S tangent to the separatrices at P_2 . The direct product of \mathfrak{S}_{E_0} with V_S and V_U generates, in the linear neighborhood of the critical point ($i = 2$) the structure of stable ($\mathfrak{S}_{E_0} \times V_S$) and unstable ($\mathfrak{S}_{E_0} \times V_U$) 3-dim tubes which coalesce, with an oscillatory approach to the tori \mathfrak{S}_{E_0} for $t \rightarrow \infty$. The energy of any orbit on these tubes is the same as that of the orbits on the tori \mathfrak{S}_{E_0} . These structures are contained in the 4-dim energy surface $H = E_0$ such that $(E_0 - E_{cr}) < 0$. We should recall that the tubes constitute a boundary for the general flow and are defined by $E_q = 0$ in the linear neighborhood of the critical point. Depending on the sign of E_q the motion will be confined inside the 4-dim tube (for $E_q < 0$) and will correspond to a flow separated from the one outside the tube (for $E_q > 0$). A detailed examination of the above motion and its extension to the nonlinear regime will be done in the next section.

The extension of our analysis beyond a linear neighborhood of critical points could be made by implementing normal forms[43, 44] and associated coordinates, modulo their radius of convergence. We will instead propose here a suitable canonical transformation which will allow us to obtain an exact analytical form for the center manifold as well as a sufficiently accurate

description of the phase space dynamics in extended regions away from the critical points. In particular we can examine the behavior of the nonlinear extensions W_S and W_U of, respectively, the linear stable ($\mathfrak{S}_{E_0} \times V_S$) and linear unstable ($\mathfrak{S}_{E_0} \times V_U$) manifolds[29] emanating from the neighborhood of the saddle-center-center P_2 . Let us introduce the canonical transformation with the generating function

$$G = (MNR)^{1/3} p_x + \frac{M}{N} p_y + \frac{MN}{R^2} p_z, \quad (47)$$

where p_x , p_y and p_z are the new momenta, resulting in

$$x = (MNR)^{1/3}, \quad y = \frac{M}{N}, \quad z = \frac{MN}{R^2}, \quad (48)$$

and

$$\begin{aligned} p_M &= \frac{1}{3} \frac{NR}{(MNR)^{2/3}} p_x + \frac{1}{N} p_y + \frac{N}{R^2} p_z, \\ p_N &= \frac{1}{3} \frac{MR}{(MNR)^{2/3}} p_x - \frac{M}{N^2} p_y + \frac{M}{R^2} p_z, \\ p_R &= \frac{1}{3} \frac{MN}{(MNR)^{2/3}} p_x - \frac{2MN}{R^3} p_z. \end{aligned} \quad (49)$$

Here, the variable x is obviously the average scale factor of the model. In these new canonical variables the equations of the invariant plane reduce to

$$y = 1, \quad z = 1, \quad p_y = 0 = p_z. \quad (50)$$

It is then clear that (x, p_x) are variables defined on the invariant plane. In these variables the phase space picture of the invariant plane is given in Fig. 1. The separatrices S emerging from the saddle-center-center P_2 separate the invariant plane in three disconnected regions, region I of oscillatory universes and regions II and III of one bounce universes. They are constituted of three branches, namely, the separatrix that divides the regions I and II and makes a homoclinic connection with the critical point P_2 and two others that approach the de Sitter asymptotic configurations for $t \rightarrow \pm\infty$. The first branch will play a fundamental role in our following discussions and will be referred to as separatrix, except where a qualification is needed to avoid confusion. The center-center-center P_1 corresponds to a stable Einstein

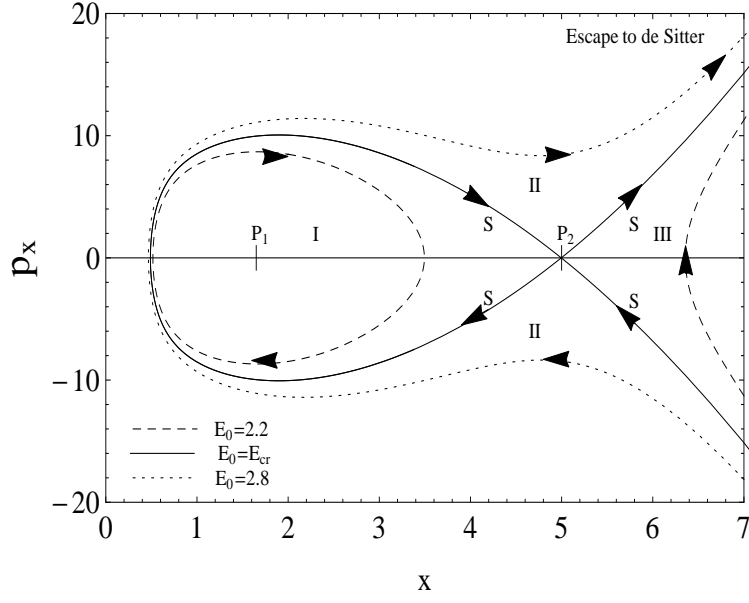


Figure 1: The phase portrait of the invariant plane for $\kappa^2 = 0.5/E_0^2$ and $\Lambda = 0.01$. The critical points P_1 and P_2 belong to the invariant plane. The separatrices S emerging from P_2 separate the plane in three disconnected regions, one of oscillatory universes the other two of one bounce universes. The separatrix dividing the regions I and II makes a homoclinic connection with P_2 . The linear neighborhood of P_2 depicts the motion of the saddle sector with V_S and V_U tangent to the separatrix at P_2 . The figure is constructed in the canonical coordinates defined in (47).

universe configuration that occurs due to the bulk-brane interaction term proportional to E_0^2 in the Hamiltonian (22).

In the variables (x, p_x, y, p_y, z, p_z) the full Hamiltonian (22) assumes the form

$$\begin{aligned} H(x, p_x, y, p_y, z, p_z; E_0) &= \frac{1}{24x} p_x^2 - \frac{y^2}{2x^3} p_y^2 \\ &- \frac{3z^2}{2x^3} p_z^2 - \frac{x}{2z^{4/3}} - \frac{1}{2} x z^{2/3} y^2 - \frac{1}{2y^2} x z^{2/3} + \frac{x}{y z^{1/3}} \\ &+ \frac{xy}{z^{1/3}} + x z^{2/3} + \frac{\kappa^2 E_0^2}{x^3} - 2\Lambda x^3 - 2E_0 = 0. \end{aligned} \quad (51)$$

We remark that the linearization of (48)-(51) about both critical points P_1 and P_2 of the dynamical system (23) yields exactly the transformation (36), and that the variables (y, p_y, z, p_z) correspond to the primed variables (K', Y', L', Z') defined on the center-center manifold S^3 about a linear neighborhood of P_2 .

The new canonical variables are most convenient since they separate the degrees of freedom of the system into pure rotational modes, (y, p_y) and (z, p_z) , and the expansion/contraction mode (x, p_x) connected to the invariant plane. This can be illustrated by implementing the expansion of the dynamical system generated from (51) about a linear neighborhood of the invariant plane, producing a linearized Hamiltonian parametrized by the variables $(x(t), p_x(t))$ describing the curves in the invariant plane, for instance, in the region I of periodic orbits bounded by the separatrix S homoclinic to P_2 . This is analogous to the usual expansion of a dynamical system about a periodic orbit. Using (51), we then obtain

$$\begin{aligned} H &= \mathcal{E}_{\text{inv}} - \frac{1}{2x^3} (p_y^2 + 3p_z^2) - x(y-1)^2 \\ &- \frac{1}{3} x(z-1)^2 = 2E_0, \end{aligned} \quad (52)$$

where

$$\mathcal{E}_{\text{inv}} = \frac{1}{24x} p_x^2 + \frac{3x}{2} + \frac{\kappa^2 E_0^2}{x^3} - 2\Lambda x^3 = \text{const.} \quad (53)$$

The resulting dynamical equations are

$$\begin{aligned}
\dot{\delta y} &= -\frac{1}{x^3} \delta p_y, \\
\dot{p}_y &= 2x \delta y, \\
\dot{\delta z} &= -\frac{3}{x^3} \delta p_z, \\
\dot{\delta p_z} &= \frac{2x}{3} \delta p_y,
\end{aligned} \tag{54}$$

where $\delta y = (y - 1)$, $\delta z = (z - 1)$, $\delta p_y = (p_y - 0)$, and $\delta p_z = (p_z - 0)$. The linearization matrix of (54) has imaginary eigenvalues $\lambda = \pm i\sqrt{2}/x(t)$, both with multiplicity two, corresponding to elliptical modes in the linear neighborhood of the invariant plane so that the motion is oscillatory about the invariant plane.

6 The non linear center manifold and the homoclinic cylinders

The nonlinear extension of the center manifold, by continuity, maintains the topology S^3 but it can no longer be decomposable into E_{rot1} and E_{rot2} so that now only the 4-dim tubes with the topology $R \times S^3$ are meaningful for the nonlinear dynamics. Similarly the extension of the structure of the 4-dim tubes away from the neighborhood of the center manifold are to be examined, and our basic interest will reside in the stable and unstable tubes, $W_S = V_S \times S^3$ and $W_U = V_U \times S^3$, that leave this neighborhood. The tubes have the structure of 4-dim spherical cylinders (of co-dimension 2), one less dimension than the energy surface, and act therefore as separatrices, separating the energy surface in two dynamically disconnected parts. The 2-dim invariant plane, defined by (29), is contained in a 6-dim phase space and it is obvious that, contrary to examples in lower dimensional systems, it does not separate the dynamics in disjoint parts. In fact the general motion about the curves of the invariant plane is an oscillatory flow confined in the interior or exterior of 4-dim tubes $R \times S^3$, so that the invariant plane (or more properly, one of the curves of the invariant plane) can be thought as a structure in the center of the tubes. This latter fact is of crucial importance

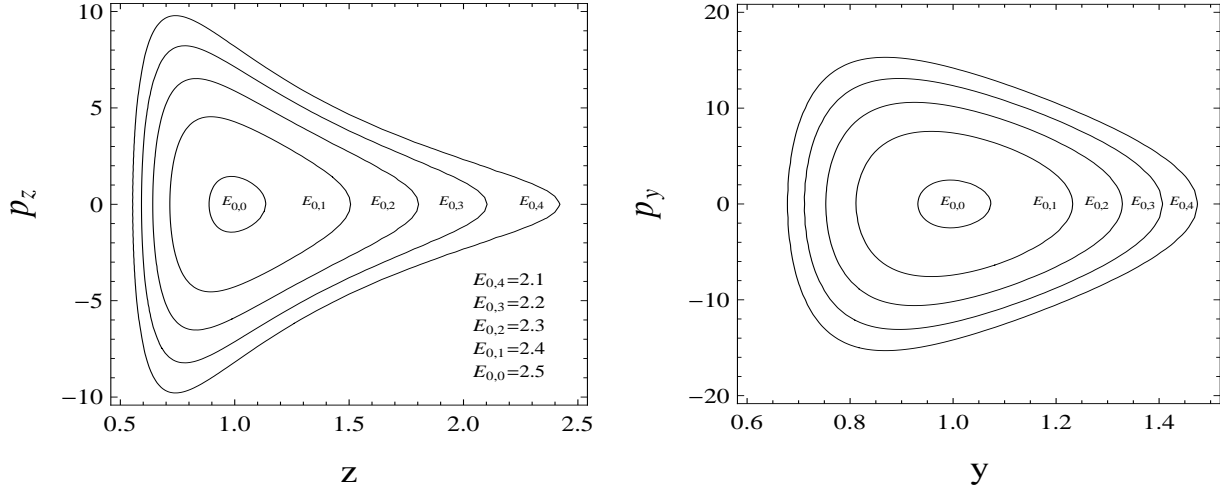


Figure 2: The sections ($y = 1, p_y = 10^{-3}$) (left panel) and ($z = 1, p_z = 0$) (right panel) of the center manifold for five values of E_0 . We note the deformation of the center manifold S^3 in the nonlinear domain as $(E_{cr} - E_{0,i})$ increases. Here $E_{cr} = 2.5127254138199464$.

in the discussion of the transversal crossing of the 4-dim cylinders W_S and W_U made in section 7.

The nonlinear extension of the center manifold in the canonical variables (y, z, p_y, p_z) is obtained by substituting $x = x_{cr}$ and $p_x = 0$ in (51), yielding after some manipulation the exact analytical expression

$$\begin{aligned}
H_c = & \frac{y^2}{2x_{cr}^3}p_y^2 + \frac{3z^2}{2x_{cr}^3}p_z^2 + x_{cr}\left(\frac{3}{2} + \frac{1}{2z^{4/3}}\right. \\
& + \frac{1}{2}z^{2/3}y^2 + \frac{z^{2/3}}{2y^2} - \frac{1}{yz^{1/3}} - \frac{y}{z^{1/3}} - z^{2/3}\Big) \\
& - \kappa^2 \frac{E_0^2 - E_{cr}^2}{x_{cr}^3} - 2(E_{cr} - E_0) = 0,
\end{aligned} \tag{55}$$

where x_{cr} and E_{cr} are respectively the coordinate and the energy of the critical point P_2 . The form (55) adopted above for the center manifold equation makes explicit its dependence on the parameter $(E_{cr} - E_0)$. For $E_0 = E_{cr}$ the center manifold reduces to the critical point. The domain of E_0 defining the center manifold satisfies the constraint to $E_0 < E_{cr}$, as already discussed; the case of the linear version (45) corresponds to $(E_{cr} - E_0)$ sufficiently small.

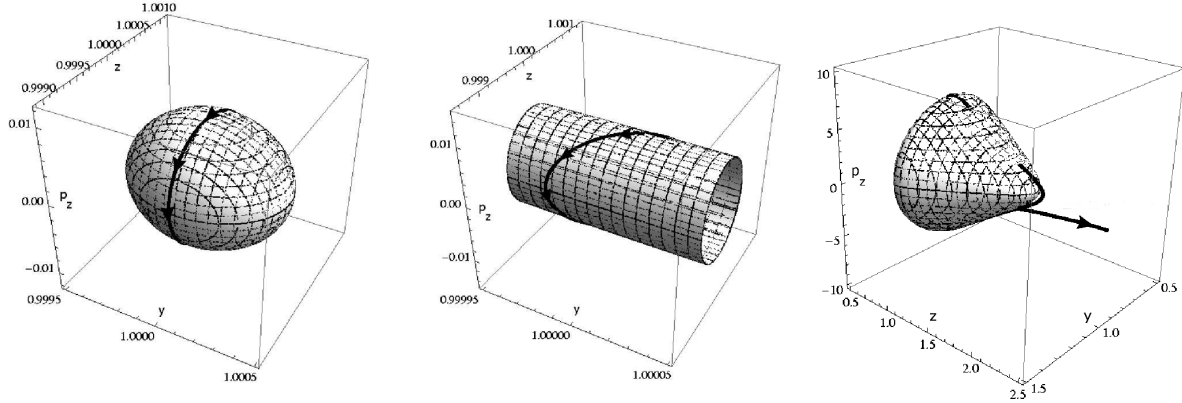


Figure 3: (left panel) The wireframe shows the 2-dim section $p_y = 10^{-3}$ of the center manifold in the space (y, z, p_z) for $E_0 = 2.512725$. The solid line indicates an orbit for $0 \leq t \lesssim 2000$ with initial conditions $(x_0 = x_{cr}, y_0 = 1, z_0 = 1, p_{x_0} = 0, p_{y_0} = 10^{-3}, p_{z_0} = 0.008177970306403768)$ on the center manifold. (middle panel) An expanded piece of the center manifold on the left, including the same orbit. (right panel) The wireframe shows the 2-dim section $p_y = 10^{-3}$ of the center manifold in the nonlinear domain, with $E_0 = 2.3$. The solid line corresponds to a one-bounce orbit which moves towards large values of z (when $t \sim 37$, $z(t) \sim 63$) before escaping to the de Sitter attractor when $t \simeq 70$. The initial condition for this orbit, $(x_0 = x_{cr}, y_0 = 1, z_0 = 1, p_{x_0} = 0, p_{y_0} = 10^{-3}, p_{z_0} = 5.879276478889785)$ is taken on center manifold. This orbit remains on the center manifold for a time up to $t \sim 12$. Here $E_{cr} = 2.5127254138199464$.

As $(E_{cr} - E_0)$ increases we have a nonlinear center manifold parametrized by the energy E_0 . In general the center manifold is a 3-dim submanifold of the 6-dim phase space contained in the 5-dim energy hypersurface $H = E_0$. In Figs. 2 we plot the sections $(y = 1, p_y = 10^{-3})$ and $(z = 1, p_z = 0)$ of the S^3 center manifold (55) showing its deformation in the nonlinear regime as the values of $(E_{cr} - E_0)$ increase. We adopted the values $\Lambda = 0.01$ and $\kappa^2 = 0.5$ so that the associated critical energy $E_{cr} = 2.5127254138199464$ and $x_{cr} = 4.974148895632555$ for the saddle-center-center P_2 . In the Figures we selected five values for E_0 .

As we have already seen the canonical coordinates (y, p_y, z, p_z) cover the center manifold S^3 and therefore we will use them not only to examine the stability of the motion restricted to S^3 but also to obtain an accurate descrip-

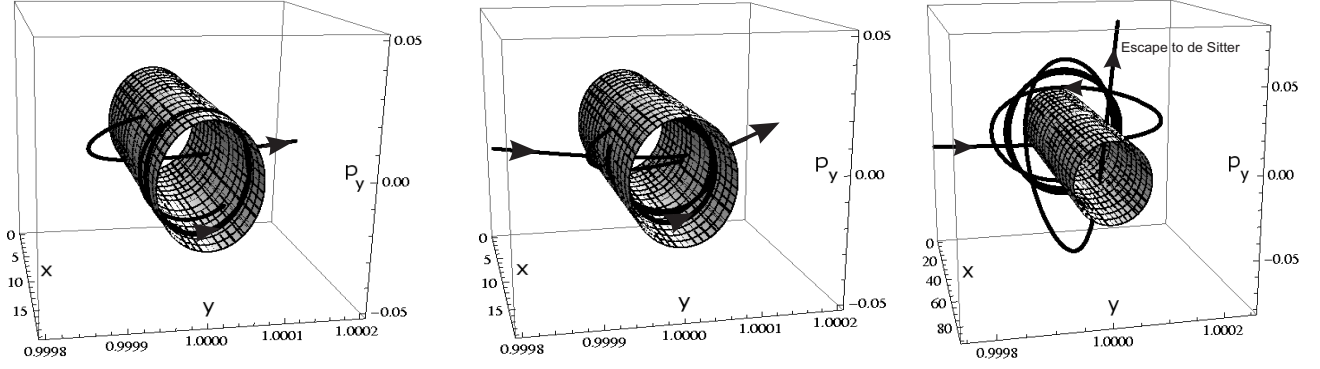


Figure 4: (left panel) The wireframe shows a piece of the 2-dim section $p_z = 0$ of the center manifold in the coordinates (x, y, p_y) for $E_0 = 7.9096539$. Here we fixed the parameters $\Lambda = 0.001$ and $\kappa^2 = 0.5$, with corresponding $E_{crit} = 7.909653935312942$. The solid line is an orbit of the full dynamics for $0 \leq t \leq 645$ with initial condition $(x_0 = x_{cr(2)}, y_0 = 1, z_0 = 1, p_{x_0} = 0, p_{y_0} = 0.023600434934712197, p_{z_0} = 0)$ taken on the center manifold. The orbit remains on the center manifold up to $t \sim 500$ when it leaves its neighborhood and is driven towards its first bounce. (middle panel) The same orbit of the left figure for $652 \leq t \leq 1320$. We can see that the orbit returns from its first bounce to a sufficiently small neighborhood of the center manifold for $t \simeq 652$, before escaping to its second bounce when $t \simeq 1320$. (right panel) The solid line indicates the same orbit of the previous figures but for $1330 \leq t \leq 2020$. This orbit returns from its second bounce to a sufficiently small neighborhood of the center manifold for $t \simeq 1330$ before escaping to the de Sitter attractor when $t \simeq 2020$.

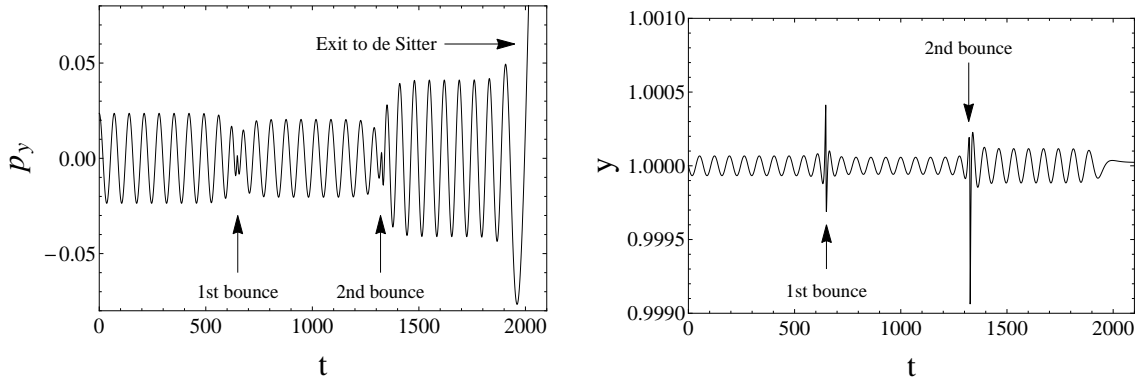


Figure 5: Plot of $p_y(t)$ and $y(t)$ corresponding to the orbit of Figs. 4 showing the typical oscillatory behavior of the rotational modes in the dynamics of the model. We note the decrease of the amplitude of $p_y(t)$ and the amplification of the conjugated $y(t)$ in a neighborhood of the bounce. This pattern is analogous for the other variables of the orbit (p_z, z) .

tion of whole the dynamics $(x(t), p_x(t), y(t), p_y(t), z(t), p_z(t))$ emerging from a neighborhood of the center manifold. In the following we will numerically illustrate this behavior. We must remark that we do not make use here of the displacing (in the direction of the unstable cylinder) of initial conditions taken on the invariant center manifold, as the shooting method in [34], but instead we make use of the instability of the motion on the center manifold which computationally conserves the Hamiltonian constraint (51) for all t . Actually in all our numerical simulations the error in the Hamiltonian constraint (51) is checked to remain $\lesssim 10^{-13}$ for the whole computational domain.

To start let us fix the parameters $\kappa^2 = 0.5$, $\Lambda = 0.01$ as in Figs. 2. In Figs. 3 we now show the 2-dim sections $p_y = 10^{-3}$ of the center manifold for $E_0 = 2.512725$ (left). The solid line indicates an orbit with initial conditions obviously satisfying (55). This orbit is evolved with the full dynamics generated from the Hamiltonian (51) and remains on the center manifold for $0 \leq t \lesssim 2000$. A piece of this center manifold is displayed in Fig. 3 (middle) where the solid line describes the same previous orbit. Fig. 3 (right) displays the section $p_y = 10^{-3}$ of the center manifold for $E_0 = 2.3$. The solid line corresponds to a one-bounce orbit which moves towards large values of z (when $t \sim 37$, $z(t) \sim 63$) before escaping to the de Sitter attractor when $t \simeq 70$.

The initial condition for this orbit is taken on the center manifold S^3 ; it remains on the center manifold up to $t \sim 12$. This increase of the dynamical instability is actually due to the large value of $(E_{crit} - E_0) \simeq 0.213$, causing the orbit to leave rapidly the center manifold towards the bounce, satisfying however the exact dynamics within an error $\lesssim 10^{-13}$.

A second set of experiments is displayed in Figs. 4 where we examined the oscillatory motion originating in the 2-dim section $p_z = 0$ of the center manifold for $\Lambda = 0.001$, $\kappa^2 = 0.5$ and $E_0 = 7.9096539$. The continuous solid line shown in the left panel is an orbit of the full dynamics for $0 \leq t \leq 645$ with the initial condition taken on the center manifold. This oscillatory orbit, which is initially periodic, remains on the center manifold up to $t \sim 500$ when it leaves this neighborhood and is driven towards its first bounce. In the middle panel the same orbit is shown for $652 \leq t \leq 1320$. We see that the orbit returns from the first bounce to a sufficiently small neighborhood of the center manifold for $t \simeq 652$ before escaping to its second bounce at $t \simeq 1320$. In the right panel we have the same orbit of the previous figures but for $1330 \leq t \leq 2020$. This orbit returns from its second bounce to a sufficiently small neighborhood of the center manifold for $t \simeq 1330$, before escaping to the de Sitter attractor when $t \simeq 2020$. These numerical simulations also reveal a typical behavior of the dynamics as we decrease E_0 . In fact the increase of $(E_{crit} - E_0)$ makes an orbit, with initial conditions taken on the center manifold, to rapidly leave this neighborhood indicating a dynamical instability (albeit the accuracy of the exact dynamics) as shown in Fig. 3 (right).

We remark that the oscillatory behavior of the orbit in the phase space sectors (y, p_y) and (z, p_z) is typical, even when the orbit tends asymptotically to one of the deSitter attractors. This is illustrated in Figs. 5 where we plot the time behavior of p_y and y of the orbit discussed in Figs. 4. We note a decrease of the amplitude of p_y and an amplification of the amplitude for the conjugated y in a neighborhood of the bounce. this pattern is analogous for the other variables (p_z, z) of the orbit.

Finally we give a numerical illustration of the stable and unstable cylinders emanating from the center manifold which are a nonlinear extension of the $\mathfrak{S}_{E_0} \times V_S$ and $\mathfrak{S}_{E_0} \times V_U$, with $\mathfrak{S}_{E_0} \subset S^3$ defined in a linear neighborhood of the saddle-center-center P_2 . We must recall that these cylinders are actually composed of orbits that have the same energy $(E_{cr} - E_0)$ of the center manifold and coalesce to it as $t \rightarrow \pm\infty$. In Fig. 6 we display the stable W_S and unstable W_U cylinders emanating from the neighborhood of the center

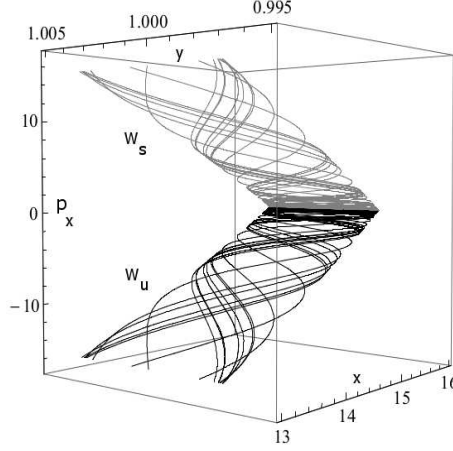


Figure 6: A numerical illustration of the unstable cylinder W_U (black) spanned by 16 orbits, with initial conditions taken on a circle in the domain (y, p_y) of the center manifold for $E_0 = 7.9096$, emerging towards the bounce. From the same domain of initial conditions the stable cylinder W_S (gray) emerges towards the bounce. The projection of the figure in the plane (x, p_x) “shadows” the separatrix of the invariant plane. Here $E_{crit} = 7.909653935312942$.

manifold towards the bounce, guided by the separatrix dividing the regions I and II of the invariant plane. We emphasize that the separatrix guiding the cylinders is actually a structure inside the cylinders. We fixed the parameters $\Lambda = 0.001$ and $\kappa^2 = 0.5$, as in Figs. 4, and took $E_0 = 7.9096$ so that $(E_{cr} - E_0) \sim 10^{-5}$.

A comment is in order now. Since the cylinders W_S and W_U are 4-dim surfaces they obviously separate the 5-dim energy surface defined by the Hamiltonian constraint (51) in two dynamically disconnected pieces, a fact that will be fundamental in the characterization of chaos in the case of an eventual transversal crossing of W_S and W_U [29, 22]. We remark that in Fig. 6 the projection of the cylinders on the plane (x, p_x) “shadows” the separatrix of the invariant plane, as expected since the separatrix is a structure contained in the interior of the two tubes. As the separatrix in question makes an homoclinic connection to the saddle-center-center critical point P_2 this fact leads necessarily to the transversal crossings of W_S and W_U , a dynamical phenomenon that we examine in the next section.

7 The transversal crossings of the cylinders and the homoclinic intersection manifold: a chaotic saddle

The results of the previous sections showed that two 4-dim cylinders, one stable $W_S = R \times S^3$ and one unstable $W_U = R \times S^3$, emerge from a neighborhood of the saddle-center-center P_2 . The center manifold S^3 is the locus of the rotational degrees of freedom of the phase space dynamics and is parametrized with the energy E_0 ($E_0 < E_{crit}$). It encloses the critical point P_2 and tends to it as $E_0 \rightarrow E_{crit}$. At this limit the cylinders W_S and W_U reduce to the separatrix S , which makes an homoclinic connection of P_2 to itself in the invariant plane. The separatrix is a structure inside the cylinders, about which the flow with the oscillatory degrees of freedom (y, p_y, z, p_z) proceeds, guiding the cylinders towards the bounce (cf. Fig.1) and leading to their eventual crossing. The first crossing is expected to occur in a neighborhood of the bounce ($x = x_b, p_x = 0$), where x_b is the scale factor of the bounce for the orbits at $p_x = 0$. In order to detect this first intersection we will adopt as the surface of section[45] the 4-dim surface $\Sigma : (x = x_b, p_x = 0)$. This first transversal crossing of the cylinders will be the main object of the present section.

Due to the conservation of the Hamiltonian constraint (51) we have that at the bounce

$$H(x = x_b, p_x = 0, y, p_y, z, p_z; E_0) = 0, \quad (56)$$

which is the equation of a closed surface with the topology of S^3 . The transversal crossing of the stable W_S and unstable W_U cylinders at the bounce will therefore be a set of points contained in the transversal intersection of two 3-spheres defined by (56), then a S^2 . These points define a set of orbits that are contained both in the stable and the unstable cylinders and are bi-asymptotic (homoclinic) to the center manifold $S^3(E_0)$. They are denoted as homoclinic points and homoclinic orbits. Therefore the set of homoclinic points has the compact support S^2 . The presence of a homoclinic orbit in the dynamics is an invariant signature of chaos in the model[27, 31]. The homoclinic intersection manifold has the topology $R \times S^2$ and consists of all homoclinic orbits biasymptotic to the center manifold. In this sense, a *chaotic saddle*[34] associated with S^3 is defined, indicating that the set of

intersection points of the cylinders has the nature of a Cantor-type set with a compact support S^2 [35].

A complete numerical study of the intersection of the 4-dim cylinders W_S and W_U is beyond the scope of the present paper (it will be considered as the subject for a future publication). Here our numerical experiments will be restricted to the dynamics on the two 4-dim invariant submanifolds of the 6-dim phase space defined by (i) $M = N$, $p_M = p_N$ (or equivalently $y = 1$, $p_y = 0$), and (ii) $N = R$, $p_N = p_R$ (or equivalently $y = z$, $p_y = 3p_z$). The denomination invariant submanifolds derives from the fact that each of them is mapped on itself by the general Hamiltonian flow (23), in other words, invariant under the flow. We will then examine the intersection of 2-dim stable and unstable cylinders in these two 4-dim invariant manifolds, according to the following experiments.

To start we fix the parameters $\kappa^2 = 0.5$, $\Lambda = 0.001$, with corresponding $E_{cr} = 7.9096539353149939$ and $x_{cr} = 15.8034567969528$. The total energy of the system is taken $E_0 = 7.9096$, so that the energy available to the rotational modes will be given by $(E_{cr} - E_0) \sim 10^{-5}$.

In the first experiment we take $(x_0 = x_{crit}, p_{x_0} = 0)$, and fix initial conditions on the 4-dim invariant submanifold (i), namely, with $(y_0 = 1, p_{y_0} = 0)$. That is, we are restricting ourselves to a particular domain of initial conditions in the sector (z, p_z) of the center manifold S^3 , which has the topology of S^1 and is defined by the Hamiltonian constraint (51) as

$$H(x = x_{cr}, p_x = 0, y = 1, p_y = 0, z, p_z) = 0.$$

By performing the evolution of orbits from a large set (of the order of 1, 500) of initial conditions in the above domain, the exact dynamics actually evolves a 4-dim invariant subset (x, p_x, z, p_z) of the full 6-dim phase space as expected due to our restriction to the 4-dim invariant manifold $(y = 1, p_y = 0)$. In this particular experiment, we have that under the exact dynamics no motion is present in the sector (y, p_y) . We generate one 2-dim stable and one 2-dim unstable cylinders of orbits which initially move towards the first bounce. In order to detect the first intersections of the two cylinders we adopt $\Sigma : (x = x_b, p_x = 0)$ as the surface of section, where $x_b \simeq 1.3118$ is the coordinate of the first bounce of the orbits at $p_x = 0$. In Fig. 7 we plot the points (z_b, p_{z_b}) of the sections of both cylinders in the first cross of Σ . The points A, B, C, D (contained in the sector (z, p_z) of Σ) characterize the transversal crossing of the cylinders. An detailed examination of the numerical points of the map

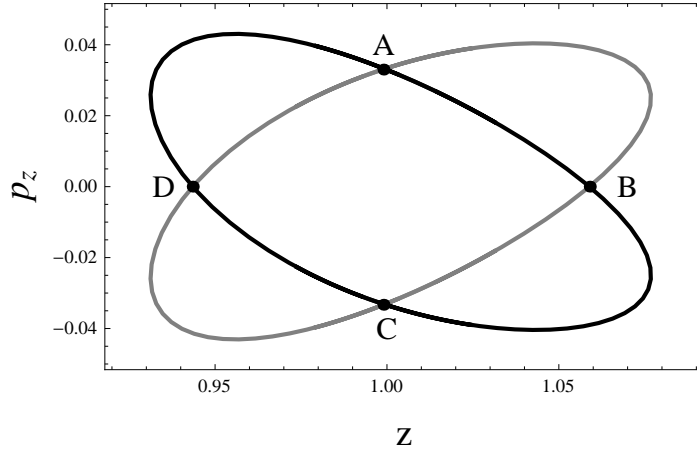


Figure 7: (first experiment) The first crossing of the stable cylinder (gray) and unstable cylinder (black) in the surface of section Σ (at the first bounce) shown in the plane (z, p_z) , for $E_0 = 7.9096$. The four points A , B , C , D are the unique points of the first transversal crossing of the cylinders. These points define homoclinic orbits which are contained in both unstable and stable cylinders and are bi-asymptotic to the center manifold $S^3(E_0)$, constituting an invariant signature of chaos in the dynamics. Here $E_{crit} = 7.909653935312942$

shows indeed that all orbits arrive at the first bounce ($x_b \simeq 1.3118, p_x = 0$) with coordinates $y_b = 1, p_{y_b} = 0$, being a further verification of the accuracy of our numerical treatment. The points A, B, C, D in Fig. 7 therefore define homoclinic orbits, namely, orbits which are in the intersection of the unstable and stable cylinders, and give an invariant characterization of chaos in the model. These homoclinic orbits are contained both in the stable cylinder and the unstable cylinder and are bi-asymptotic to the center manifold $\mathfrak{S}_{E_0} \subset S^3(E_0)$.

The coordinates (y, p_y, z, p_z) of the homoclinic points A, B, C, D are given approximately by

$$\begin{aligned} A &\simeq (1, 0, 0.9997818, 0.0330003), \\ B &\simeq (1, 0, 1.0604379, 0.0012771), \\ C &\simeq (1, 0, 0.9991485, -0.0331563), \\ D &\simeq (1, 0, 0.9445269, -0.0011262). \end{aligned} \tag{57}$$

Analogously in the second experiment we maintain the same values for the parameters E_0, κ^2 and Λ together with the initial conditions ($x_0 = x_{crit}, p_{x_0} = 0$). However now fix the remaining initial conditions on the 4-dim invariant submanifold (ii) instead, namely, $(y_0 = z_0, p_{y_0} = 3p_{z_0})$. In fact we are restricting ourselves to a particular domain of initial conditions of the center manifold S^3 which has the topology of S^1 and is defined by the Hamiltonian constraint

$$H(x = x_{cr}, p_x = 0, y = z, p_y = 3p_z) = 0.$$

With the exact dynamics we generate one 2-dim stable and one 2-dim unstable cylinders which initially move towards the first bounce. These cylinders are generated from a set of about 1,500 orbits, with initial conditions taken in the above domain which actually correspond to a flow in the 4-dim invariant submanifold (ii) of the full 6-dim phase space.

In Fig. 8 we plot the points (z_b, p_{z_b}) of the sections of both cylinders in the first crossing of Σ . The four points E, F, G, H of the figure characterize the transversal crossing of the cylinders, defining homoclinic orbits which are in the intersection of the unstable and stable cylinders and are bi-asymptotic to the center manifold $\mathfrak{S}_{E_0} \subset S^3(E_0)$. A complementary map in the sector

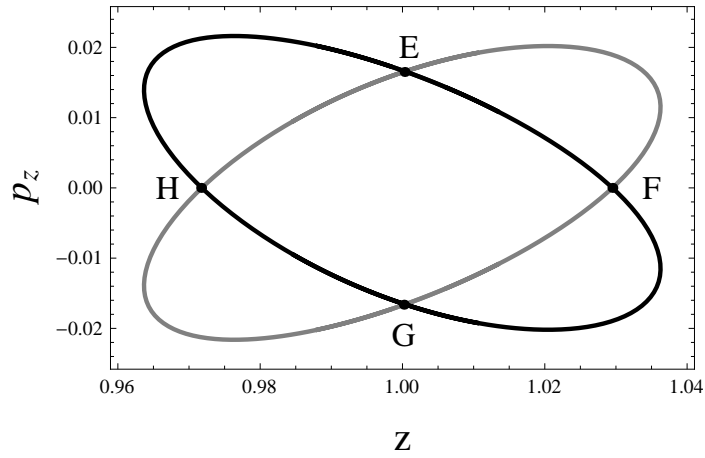


Figure 8: (second experiment) Projection on the plane (z, p_z) of the first crossing of the stable cylinder (gray) and unstable cylinder (black) in the surface of section Σ (at the first bounce). In this projection the four points E , F , G , H are the unique points of the first transversal crossing of the cylinders (cf. text). These points define homoclinic orbits which are contained in both unstable and stable cylinders and are bi-asymptotic to the center manifold $S^3(E_0)$, constituting an invariant signature of chaos in the dynamics of the model.

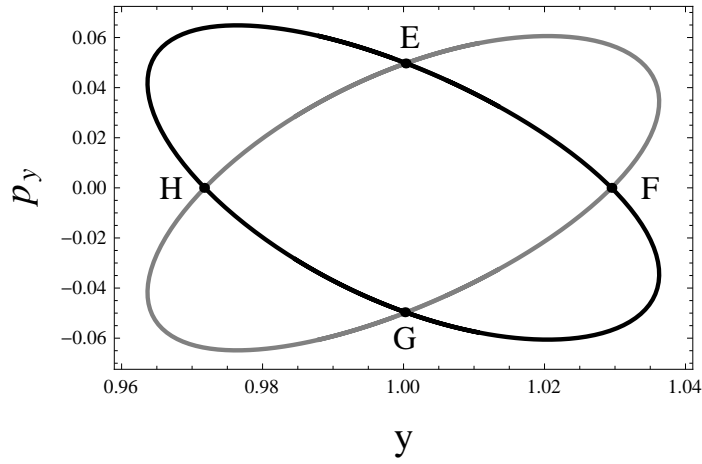


Figure 9: (second experiment) Projections on the complementary plane (y, p_y) showing the first crossing of the stable cylinder (gray) and unstable cylinder (black) in the surface of section Σ (at the first bounce). The four points E, F, G, H of figure 8, characterizing the transversal crossing of the cylinders are shown, constituting an invariant signature of chaos in the dynamics of the model.

(y, p_y) is given in Fig. 9, showing the first crossing of the cylinders by surface of section Σ at the bounce. This map confirms the transversal crossings at the points E, F, G, H . The coordinates (y, p_y, z, p_z) of the homoclinic points E, F, G, H are given approximately by

$$\begin{aligned}
E &\simeq (1.0002743, 0.0496506, 1.0002743, 0.0165502), \\
F &\simeq (1.0290076, -0.0013846, 1.0290076, -0.0004615), \\
G &\simeq (1.0002743, -0.0496506, 1.0002743, -0.0165502), \\
H &\simeq (0.9721427, -0.0009974, 0.9721427, -0.0003324).
\end{aligned}
\tag{58}$$

An detailed examination of the numerical points of the map shows that all orbits arrive at the first bounce ($x \simeq 1.3118, p_x = 0$) with coordinates $(y_b = z_b)$ and $(p_{y_b} = 3p_{z_b})$. This is also illustrated in Figs. 10 where the first crossing of the unstable and stable cylinders with the surface of section Σ in the bounce are displayed. The section of both cylinders, projected on the sectors (y, z) and (p_y, p_z) , lie on the straight lines $y = z$ and $p_y = 3p_z$ respectively, as expected. This is also a further verification of the accuracy of our numerical results.

The sets (57) and (58) are two distinct numerical evidences of chaos in the dynamics, and constitute an invariant signature of chaos in the model. We must mention that the dynamics near homoclinic orbits is very complex associated with the presence of horseshoe structures[28, 27, 29, 22, 46]. The coordinates of the homoclinic points (57) and (58) satisfy the constraint (56), implying that they are contained in the transversal intersection of two S^3 at the bounce, namely, a S^2 . This fact indicates that the *chaotic saddle* – connected with the structure of homoclinic orbits bi-asymptotic to the center manifold S^3 – is a Cantor-type set having the compact support S^2 [35].

8 Conclusions and final comments

In this paper we examined the dynamics of a Bianchi IX model, with three scale factors, sourced by a pressureless perfect fluid in the framework of bouncing Braneworld cosmology. Assuming a timelike extra dimension and a 5-D de Sitter bulk, the modified Einstein's field equations on the 4-dim Lorentzian brane furnish a dynamics with correction terms that avoid the singularity and implement nonsingular bounces in the early phase of the

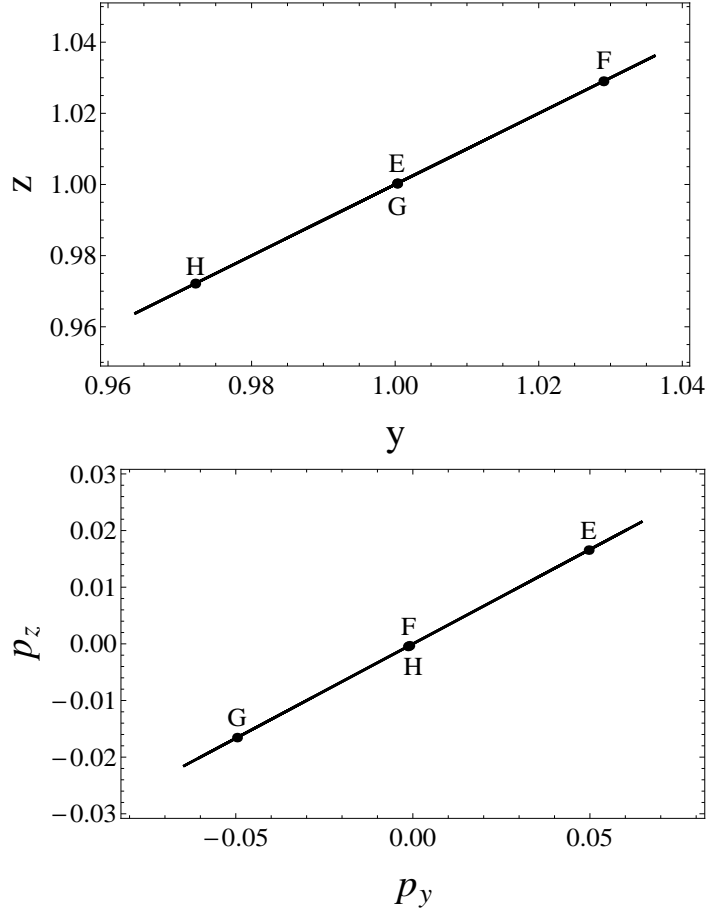


Figure 10: The first crossing of the stable and unstable cylinders with the surface of section Σ , projected on the phase space sections (y, z) and (p_y, p_z) . As expected the sections of both cylinders coincide on the straight lines $y = z$ and $p_y = 3p_z$. The points corresponding to the transversal crossing of the cylinders E , F , G and H are plotted for reference.

universe. In terms of metric functions the modified Einstein's equations have a first integral that can be expressed as a Hamiltonian constraint in a 6-dim phase space, yielding a three degrees of freedom dynamical system which governs the motion in phase space. Due to an effective cosmological constant on the brane the phase space presents two critical points in a finite region of the phase space, a center-center-center and a saddle-center-center, plus two critical points at infinity corresponding to the de Sitter solution. Together with a 2-dim invariant plane of the dynamics the critical points allow to organize the dynamics of the phase space.

We examine the structure of the dynamics in a linearized neighborhood of the saddle-center-center. We identify constants of motion associated with the saddle sector, which allow to define the linear stable V_S and unstable V_U manifolds. We also identify constants of motion connected to the center-center sector, which define the center manifold of linearized unstable periodic orbits and has the topology of S^3 . In the linear domain the direct product $V_S \times S^3$ and $V_U \times S^3$ define the structure of stable and unstable cylinders which constitute boundaries in the 5-dim energy surface of the dynamics.

The nonlinear extension of the center manifold of unstable periodic orbits is parametrized by the constant of motion E_0 ($E_0 < E_{cr}$) with the topology of S^3 maintained. As one decreases the parameter E_0 the nonlinearity of the center manifold increases, with a corresponding increasing of the dynamical instability as shown in our numerical simulations. The extension of the 4-dim stable $W_S = V_S \times S^3$ and unstable $W_U = V_U \times S^3$ cylinders away from the neighborhood of the center manifold have the structure of 4-dim spherical cylinders with the topology $R \times S^3$.

By a proper canonical transformation we are able to separate the three degrees of freedom of the dynamics into one degree – connected with the expansion and/or contraction of the scales of the model – isolated from the other two related to pure rotational degrees of freedom associated with the center manifold S^3 . By expanding the Hamiltonian constraint and Hamilton's equations in these coordinates we show that the typical dynamical flow is an oscillatory mode about the orbits of the invariant plane. In particular the stable W_S and unstable W_U cylinders are composed of oscillatory orbits about the separatrices which emerge from the saddle-center-center critical point and guide the cylinders. These cylinders have the same energy E_0 of the center manifold and coalesce to it as $t \rightarrow \pm\infty$. As these spherical cylinders are 4-dim surfaces they separate the 5-dim energy surface in two dynamically disconnected pieces. This fact is a fundamental feature of the dynamics for

characterization of chaos in the case of an eventual transversal intersection of W_S and W_U . As the separatrix which divides regions I and II in the invariant plane makes an homoclinic connection to the saddle-center-center critical point, this fact necessarily leads to the transversal crossings of W_S and W_U . The transversal crossing of the cylinders consists of homoclinic orbits which are contained both in the stable and the unstable cylinder and are biasymptotic to the center manifold S^3 . The presence of a homoclinic orbit in the dynamics is an invariant signature of chaos in the model[28, 27, 23, 31]. The homoclinic intersection manifold has the topology of $R \times S^2$ and consists of all homoclinic orbits biasymptotic to the center manifold defining a *chaotic saddle*[34] associated with S^3 .

The first transversal crossings of the stable W_S and unstable W_U cylinders are shown numerically in two distinct experiments. For the sake of computational simplicity we restricted ourselves to cylinders generated from initial conditions taken on the center manifolds of the two 4-dim invariant manifolds of the dynamics defined respectively by $(y = 1, p_y = 0)$, and $(y = z, p_y = 3p_z)$. We adopted the surface of section Σ at the bounce defined by $(x_b, p_x = 0)$ where x_b is the scale factor of the bounce for the orbits. By performing the evolution of orbits via the 6-dim exact dynamics we generate one 2-dim stable and one 2-dim unstable cylinders of orbits, and detected their transversal intersection corresponding to four homoclinic points in the first crossing of Σ by the cylinders, for both experiments. These points define orbits which are homoclinic to the center manifold $\mathfrak{S}_{E_0} \subset S^3(E_0)$.

In all our numerical simulations we used the 6-dim exact dynamics, in accordance with (23), and the error in the Hamiltonian constraint (51) is checked to remain $\lesssim 10^{-13}$ for all t .

We finally compare some features of the dynamics, namely the oscillatory approach to the bounce and the chaotic behavior of the dynamics, with analogous features present in the BKL conjecture in general relativity. First we note that in both models the oscillatory approach to the bounce/singularity is a key feature of the dynamics. In the general Bianchi IX model discussed here the three degrees of freedom of the dynamics are separated into one degree (connected with the expansion and/or contraction of the scales of the model) plus pure rotational degrees of freedom associated with the center manifold S^3 . The typical dynamical flow is an oscillatory mode about the orbits of the 2-dim invariant plane; in particular from the center manifold it emerges the stable and unstable 4-dim cylinders of oscillatory orbits that are guided towards the bounce by the separatrix in the invariant plane. In

the limit of $\kappa^2 \rightarrow 0$ (close to the general relativity dynamics) the motion on, or about the unstable cylinder approximates the oscillatory BKL motion up to a scale $x^3 \geq \kappa^2$. As one can make κ^2 as small as wanted, a long oscillatory approach towards a neighborhood of $x = 0$ can be developed, with a behavior analogous to one of the Kasner eras of the BKL model. However κ^2 cannot be made equal to zero as this would correspond to a change of topology of the phase space. The same considerations would apply for the case of a mixmaster universe, with a nonvanishing cosmological constant and $E_0 = 0$, in general relativity. Second, the chaos in the present model has a homoclinic origin, resulting from the homoclinic transversal intersections of the stable and unstable 4-dim cylinders emerging from the center manifold S^3 . In contrast the chaotic behavior in the BKL dynamics appears in a map that connects the length of the succeeding Kasner eras in the approach to the singularity of general relativity, for which we have no counterpart. Nevertheless, considering the general relativity limit, we have topological evidence that the 4-dim cylinders – emerging from the center manifold S^3 and guided by the separatrix connecting the saddle-center-center to the singularity – should intersect and generate a homoclinic orbit from this intersection.

In a future work we intend to examine the transversal intersection of the spherical cylinders $R \times S^3$ in the full 6-dim phase space. We also intend to examine the chaotic exit to the final accelerated de Sitter stage for initial condition sets (corresponding to initially expanding universes) taken in a small neighborhood about the separatrix S approaching the saddle-center-center for $t > 0$. As in [13], we expect these sets to have fractal basin boundaries connected to the code recollapse/escape leading to a chaotic exit to the de Sitter accelerated phase. We also expect to observe the draining of initial condition basins from recollapse to escape behavior, as time increases. For $t \rightarrow \infty$ only the homoclinic intersection manifold is expected to remain in recurrent oscillatory motion.

Acknowledgements

RM acknowledges the financial support from CNPq/MCTI-Brasil and CAPES-FAPERJ, through a PCI-BEV research grant No. 170047/2014-8 and Post-Doctoral grant No. 101.493/2014, respectively. IDS acknowledges the financial support from CNPq/MCTI-Brasil, through a research grant No. 304064/2013-0. EVT acknowledges FAPES-ES-Brazil. The figures were gen-

erated using the Wolfram Mathematica 7.

References

- [1] V. A. Belinskii, I. M. Khalatnikov and E. M. Lifshitz, Adv. Phys. 19, 525 (1970);
- [2] I. M. Khalatnikov and E. M. Lifshitz, Phys. Rev. Lett. 24, 76 (1970);
- [3] V. A. Belinskii, I. M. Khalatnikov and E. M. Lifshitz, Adv. Phys. 31, 639 (1982).
- [4] E. M. Lifshitz, I. M. Lifshitz and I. M. Khalatnikov, JETP 59, 322 (1970);
- [5] I. M. Khalatnikov, E. M. Lifshitz, K. M. Khanin, L. N. Shchur and Ya. G. Sinai, J. Stat. Phys. 38, 97 (1985).
- [6] R. M. Wald, *General Relativity* (University of Chicago Press, Chicago, 1984).
- [7] M. Bojowald (Loop Quantum Cosmology Collaboration), Living Rev. Relativity 8, 11 (2002), <http://relativity.livingreviews.org/Articles/lrr-2005/11>; M. Bojowald and R. Tavakol, arXiv:gr-qc/08024274.
- [8] K. R. Dienes, *String theory and the path to unification: a review of recent developments*, Phys. Rep. 287, 447-525 (1997); M. Kaku, *Strings, Conformal fields and M-theory*, Springer-Verlag, New York (2000); C. Rovelli, *Loop quantum gravity*, Living Rev. Rel. 1, 1-34 (1998).
- [9] T. Shiromizu, K. Maeda and M. Sasaki, Phys. Rev. **D62**, 024012 (2000).
- [10] Y. V. Shtanov, hep-th/0005193 (2000); Y. V. Shtanov, Phys. Lett. B541, 177 (2002); Yu. Shtanov and V. Sahni, Phys. Lett. B557, 1 (2003).
- [11] R. Maartens, Phys. Rev. **D62**, 084023 (2000); Living Rev. Rel. 7:7,2004 (gr-qc/0312059).
- [12] Rodrigo Maier, Ivano Damião Soares and Nelson Pinto-Neto, Phys. Rev. D 87, 043528 (2013).
- [13] R. Maier, I. Damião Soares and E. V. Tonini, Phys. Rev. **D79**, 023522 (2009).
- [14] A.D. Sakharov, Zh. Eksp. Teor. Fiz. 87, 375 (1984) [Sov. Phys. JETP 60, 214 (1984)]; J. Barrett, G. W. Gibbons, M. J. Perry, C. N. Pope and P. J. Ruback, Int. J. Mod. Phys. A9, 1457 (1994).

- [15] Ya. Arefeva, B.G. Dragovic and I.V. Volovich, Phys. Lett. B177, 357 (1986).
- [16] M. Chaichian and A. B. Kobakhidze, Phys. Lett. B488, 117 (2000).
- [17] Ya. Arefeva and I.V. Volovich, Phys. Lett. B164, 287 (1985).
- [18] G.R. Dvali, G. Gabadadze, G. Senjanovic, in Many Faces of the Superworld: Yuri Golfand Memorial Volume 525- 532, Eds. Y. Golfand, M. Shifman, M.A. Shifman (World Scientific, 1999).
- [19] F. J. Yndurain, Phys. Lett. B256, 15 (1991).
- [20] A. Iglesias, Z. Kakushadze, Phys. Lett. B515, 477 (2001).
- [21] M. Berry, *Regular and Irregular Motion* in Topics on Linear Dynamics, AIP Conf. Proc. 46, 16-120 (1978).
- [22] J. Guckenheimer and P. Holmes, *Dynamical Systems and Bifurcations of Vector Fields* (Springer-Verlag, New York, 1983).
- [23] C. Conley, Journ. Diff. Eqns 5, pp 136-158 (1969).
- [24] C. Grotta-Ragazzo, Comm. Pure App. Math. 50, 2, pp 105-147 (1997).
- [25] C. Grotta-Ragazzo, Comm. Math. Phys. 184, 2, pp 251-272 (1997).
- [26] J. Llibre, R. Martinez, C. Simó, Jour. Diff. Eqns. 58, pp. 104-156 (1985).
- [27] J. K. Moser, *Stable and Random Motions in Dynamical Systems* (Princeton University Press, Princeton, 1973).
- [28] S. Smale, Bull. Amer. Math. Soc. 73, 747-817 (1967).
- [29] S. Wiggins, *Global Bifurcations and Chaos* (Springer-Verlag, 1988).
- [30] S. Wiggins, *Normally Hyperbolic Invariant Manifolds in Dynamical Systems* (Springer, 1994)
- [31] S. Wiggins, *Introduction to Applied Nonlinear Dynamical Systems and Chaos* (Springer, 2003)
- [32] H. E. Nusse and J. A. Yorke Physica D, 36, 137 (1989).
- [33] H. Waalkens and S. Wiggins, Regular and Chaotic Dynamics, 15, 1, pp. 139 (2010).
- [34] H. Waalkens, A. Burbanks and S. Wiggins, J. Phys. A: Math. Gen. 37 L257L265 (2004).
- [35] J. Cresson J. Diff. Eqns. 187 269 (2003).

- [36] L. P. Eisenhart, *Riemannian Geometry* (Princeton University Press, New Jersey, 1997).
- [37] A. H. Taub, *Phys. Rev.* **94**, 6 (1954).
- [38] W. Israel, *Il Nuovo Cimento* **44B**, 1 (1966).
- [39] H. P. de Oliveira, A. M. Ozorio de Almeida, I. Damião Soares and E. V. Tonini, *Phys.Rev.* D65 083511 (2002).
- [40] C. L. Siegel and J. K. Moser, *Lectures on celestial Mecahnics* (Springer Verlag, Berlin, 1971).
- [41] H. V. McIntosh, *Am. J. Phys.* 27, 620 (1959).
- [42] D. M. Y. Sommerville, *The Elements of Non-Euclidean Geometry* (Dover, New York, 1958).
- [43] V. I. Arnold, V. V. Kozlov, and A. I. Neishtadt, *Mathematical Aspects of Classical and Celestial Mechanics in Dynamical Systems* vol. 3, (Springer, 1988).
- [44] J. Murdock, *Normal Forms and Unfoldings for Local Dynamical Systems*, (Springer, 2003).
- [45] A. J. Lichtenberg and M. A. Lieberman *Regular and Chaotic Dynamics*, (Springer Science, 1992).
- [46] A. M. Ozorio de Almeida, *Hamiltonian Systems, Chaos and Quantization* (Cambridge University Press, Cambridge, 1993).